https://doi.org/10.5194/egusphere-2026-2590
Preprint. Discussion started: 27 May 2026

Technical Note: Reducing age dispersion in in-situ (U-Th)/He dating: How to optimize ablation pit geometries with OptiPit

Hagen Hoemann[1], Mathias Hueck[1], István Dunkl[2]

[1] Institute of Geosciences, Ruhr-University, Bochum, 44801, Germany
[2] Geoscience Center, Georg-August-University, Göttingen, 37077, Germany

Correspondence to: Hagen Hoemann (hagen.hoemann@ruhr-uni-bochum.de)

Abstract. Radiometric dating requires the measurement of related parent and daughter isotopes to produce meaningful ages. The alpha ejection during the decay of uranium and thorium spatially separates the parent and daughter nuclides analysed in (U-Th)/He dating by a few tens of microns within the crystals. In-situ (U-Th)/He dating applies two superimposed laser ablation spots to analyse the liberated parent and daughter nuclides sequentially, assuming that the analysed He is derived from the analysed U and Th. However, computer simulation considering alpha ejection visualizes the helium-source volume around the helium-pit and reveals that in-situ (U-Th)/He dating undermines that assumption. Only a fraction of the parent nuclei that produced the measured volume of helium are probed during analysis. Furthermore, while those parent nuclei contribute equally to the analysed radionuclide budget, their contribution to the helium budget is a complex function depending on the relative location of the alpha emitter to the laser ablation spots, as well as the geometry of the latter. This geometry controls the overdispersion of in-situ (U-Th)/He ages produced by radionuclide zonation, which can be reduced to a minimum by optimizing the geometries. This contribution serves as a guideline on how to minimize age overdispersion produced by the interplay of radionuclide zonation and the geometry of the laser ablation spots and demonstrates how to assess the reliability of in-situ (U-Th)/He ages by optimizing the laser pit geometry.

1. Introduction

Intracrystalline entrapment of radiogenic He emitted by alpha decay of radioactive uranium, thorium, and samarium isotopes is the basis of (U-Th)/He dating (e.g. Farley 2002; Reiners 2005). The isotopic system is analysed in a variety of minerals, of which zircon, apatite, and titanite are most commonly used to address thermochronological questions (e.g. Baughman & Flowers 2020; Hueck et al. 2018). (U-Th)/He analysis is conventionally carried out by degassing entire crystals or crystal fragments in a vacuum chamber to quantify the total amount of He. After measuring the dimensions of the degassed grain to correct for He losses due to alpha ejection (Farley et al. 1996), it is completely dissolved in acid to analyse its bulk U, Th, and Sm content through isotope dilution using ICP-MS. Conventional (U-Th)/He dating, however, suffers from age overdispersion produced by inclusions (Ehlers & Farley 2003;

https://doi.org/10.5194/egusphere-2026-2590
Preprint. Discussion started: 27 May 2026

Danišík et al. 2017), radionuclide zonation (Farley et al. 1996; Farley 2002; Hourigan et al. 2005), He implantation from neighbouring phases in low-eU minerals (Spiegel et al. 2009), and grain fragmentation which hinders F_T correction (Brown et al. 2013). The complications caused by inclusions and grain fragmentation are usually addressed by an uncompromising pre-selection process. This process, however, reduces the number of grains available for dating and introduces bias into detrital age populations (Malusà et al. 2013; Léger et al. 2023). The conventional, bulk-crystal procedure averages out any chemical zonation present in the analysed material despite it being a significant source of error in the (U-Th)/He system (Fitzgerald et al. 2006; Dobson et al. 2008; Flowers et al. 2023).

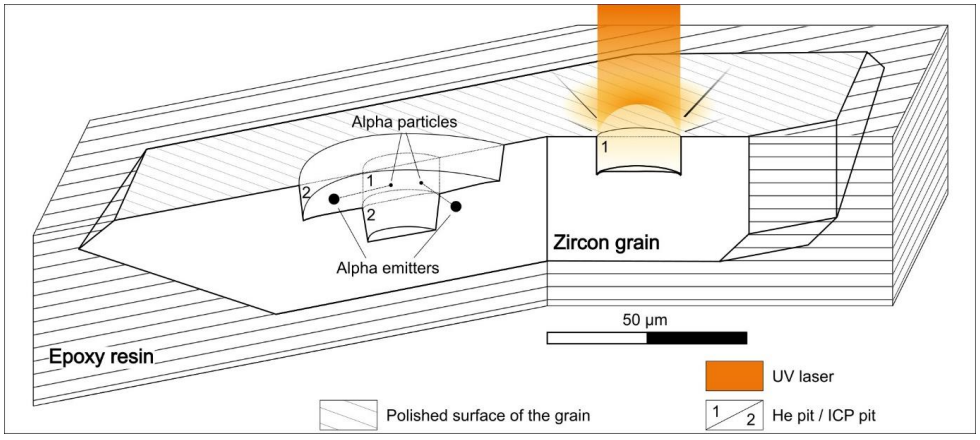

Figure 1: Block diagram showing a mounted and polished zircon crystal and the laser ablation steps of in-situ (U-Th)/He dating. At first, a small pit (1) is ablated and the liberated radiogenic helium is measured by a noble-gas mass spectrometer. The concentrations of alpha-emitting elements are determined by a second ablation step. This pit is placed concentrically over the first one (ICP pit, 2).

Laser-ablation (U-Th)/He dating (referred to as “in-situ (U-Th)/He dating”) has been developed to mitigate those sources of bias (Boyce et al. 2006; Glotzbach & Ehlers 2024). The current method usually involves mounting entire crystals or fragments in a mount, which is polished to the depth of at least 15 µm to expose an inner surface. After an optional step of structural and compositional mapping using cathodoluminescence and/or BSE imaging and/or Raman spectroscopy, He is extracted from laser pits ablated from the exposed inner surface (He pit, Fig. 1). These usually have radii of about 7 to 30 µm at depths of 2 to 20 µm. Thereafter, the volume of the He pit is measured using atomic force microscopy (AFM) or a confocal laser microscope to calculate the He concentration within the ablated material. The concentrations of the radioactive parent elements U, Th, and Sm are subsequently measured from material ablated from the same location, ablated from either a bigger or smaller area (typically with radii smaller than 35 µm at depths similar to the He pit), which is assumed to be representative of the source of the measured He (ICP pit, Fig. 1).

The in-situ dating is favoured in the advanced provenance analysis, as this procedure can yield as “by product” also the U-Pb age of the dated grain serving U-Pb-He double-dating results, e.g. both emplacement and low-T ages (e.g. Horne et al. 2016; Dunkl et al. 2024). Additionally, the in-situ (U-Th)/He dating has some major advantages over conventional, entire grain (U-Th)/He dating. (i) There is the possibility to visualize the compositional and structural zoning across the polished grains, which

https://doi.org/10.5194/egusphere-2026-2590
Preprint. Discussion started: 27 May 2026

enables the contextualization of zonation with the He age and the selection of areas suitable for dating within complexly zoned crystals. This is especially important in old and radionuclide-rich zircons which experience a significant reduction in He retentivity due to radioactive damage accumulation (e.g. Guenthner et al. 2013), which can render the production of meaningful He ages impossible in some samples.

(ii) In-situ dating allows the removal of bias introduced into the age population by restrictive pre-selection of grains. Because only a portion of the crystal is analysed, it is possible to also consider inclusion-bearing and anhedral grains into the analysis, which are not datable by the conventional technique. (iii) If the in-situ dating is performed more than one alpha stopping distance away from the grain boundaries, the technique does not require alpha ejection correction (F_t correction) that has the highest contribution to the total uncertainty of the conventional He ages (e.g. Farley et al. 1996; Fitzgerald et al. 2006; Flowers et al. 2023; Glotzbach & Ehlers 2024). (iv) The in-situ dating has considerably higher throughput than the conventional technique and (v) it does not require using the toxic and time-consuming HF-based digestion and the multi-step chemical procedure.

While in-situ (U-Th)/He dating alleviates the need for F_t correction this does not mean that the method is insensitive to the alpha ejection inherent to (U-Th)/He dating. Contrary even, considering alpha stopping distances becomes more important. The scale of the laser ablation pits, which lie in the range of a few tens of micrometres, is the same as the alpha stopping distances in commonly dated accessory minerals, which range from 11 to 29 µm in zircon. This means that the He present in each location within the crystal must have been implanted into its current location from the surroundings (Fig. 1). The parent isotopes that produced the He measured within the He pit, herein referred as “productive parents”, are not necessarily probed by the ICP pit, or they contribute only a minor fraction to the bulk of measured U, Th, and Sm. This undermines the fundamental geochronological assumption that the measured He is genetically linked to the measured parent isotopes. Thus, in-situ (U-Th)/He dating necessarily introduces the risk of overdispersion in the He age population for all crystals that are not perfectly homogeneous.

This risk necessitates a solution which can quantify the overdispersion produced by the misrepresentation of the measured parent and daughter nuclei. Previous authors have noted this problem when publishing in-situ (U-Th)/He data. For example, Horne et al. (2016) argue that a genetic link between parent and daughter isotopes is established if the size of the ICP pit envelops the He pit enough to capture all alpha-emitting parents which may have contributed He to the total budget within the He pit. They therefore drilled ICP pits which exceed the radius and depth of each He pit by about 20 µm. Contrasting to this, Evans et al. (2015) opted for ablating He pits less than 1 µm deep and about 60 µm in diameter, into which a deeper ICP pit with a radius much smaller than 60 µm is being shot. The strong contrast in these two illustrative approaches demonstrates the importance of a theoretical foundation to quantify the genetic link between parent and daughter isotopes and judge the quality of a measurement. This link is necessary not only for optimizing pit geometries, but also to account for the impact of not uniformly distributed parent nuclides in the vicinity of the in-situ pits into the resulting (U-Th)/He date. This contribution therefore aims to lay the theoretical groundwork and provide a guideline

https://doi.org/10.5194/egusphere-2026-2590
Preprint. Discussion started: 27 May 2026

of how to judge and optimize the geometries of laser ablation pits for future studies using in-situ (U-Th)/He dating.

2. Method

2.1 Significance of alpha ejection in in-situ (U-Th)/He dating

Each step in the decay chains of ^{238}U, ^{235}U, and ^{232}Th releases alpha particles between 4 and 8 MeV of energy (Farley et al. 1996; Ketcham et al. 2011). More than 98% of this energy is released as the kinetic energy of the alpha particle, while the rest of the energy is conserved in the recoil of the much heavier daughter nucleus (Belyaev & Ross 2021). Consequently, the heavy daughter nucleus is displaced over only 30 to 40 nm, being stopped by nuclear interactions with the crystal lattice (Jonckheere und Gögen 2001). However, the much lighter alpha particle is ejected into a random direction. Initially only slowed by electronic interactions with the atoms of the crystal lattice, it travels for distances of about 10 to 34 µm in the usually dated minerals before coming to rest (Jonckheere und Gögen 2001; Farley et al. 1996). These stopping distances, also called “range”, consequently allow to simplify the spatial distribution of alpha particles around an emitter at location X as spheres centred around X, which have

https://doi.org/10.5194/egusphere-2026-2590
Preprint. Discussion started: 27 May 2026

the radii of the alpha stopping distances of the decay chain (e.g. Farley et al. 1996; Glotzbach und Ehlers 2024).

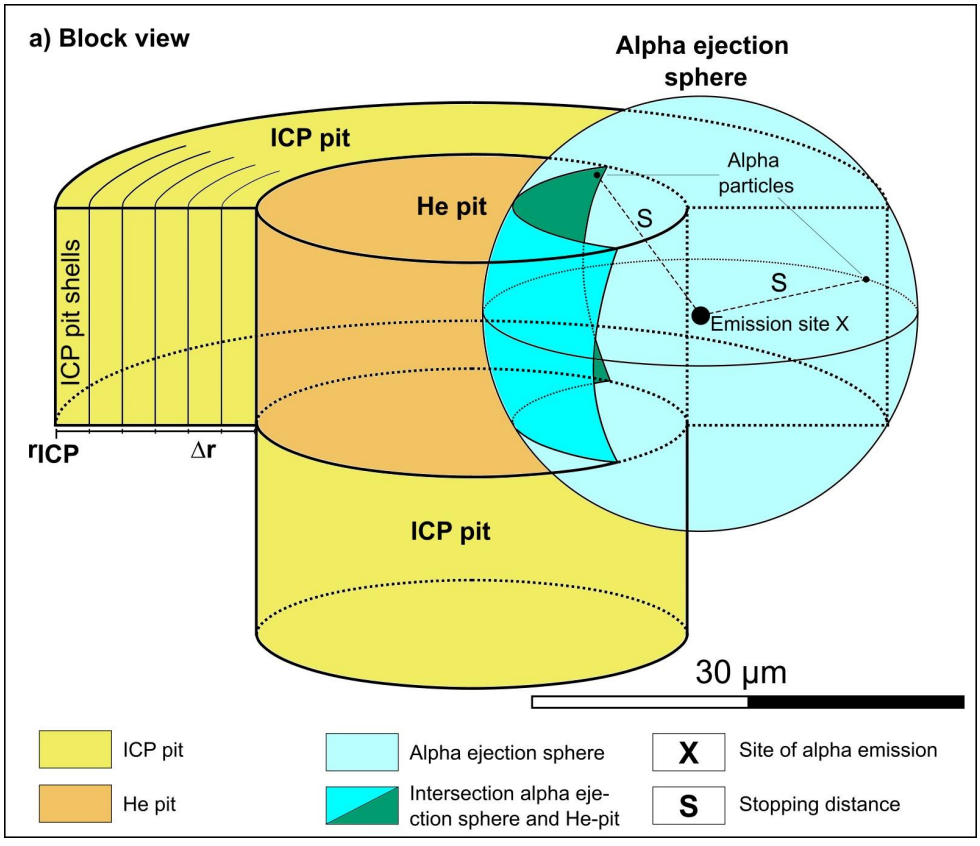

Figure 2: Schematic block view of the in-situ laser ablation pits shown in Fig. 1 compared to the size of the average alpha ejection sphere for ^{238}U in zircon. For calculation purposes, the ICP pit can be subdivided into shells of equal thickness which increase in volume from the centre of the ICP pit to its outermost shell (see Fig. 3).

In the case of He particles quantified during in-situ (U-Th)/He dating, those alpha emission spheres intersect the He pit ablated into the crystal, which itself can be approximated by a cylinder (Fig. 2). Then, the intersection area between both geometrical bodies divided by the total surface of the sphere represents the probability of an alpha particle to be implanted into the He pit. This probability evidently depends on the relative position of the sphere and the cylinder to each other, as this will impact the intersection area of both bodies, or, in other words, the implantation of the He atom within the volume of the He pit. For example, if the emission location in Fig. 2 is moved horizontally away from the He pit, the intersection area shrinks, and so does the probability of alpha particles to be implanted inside the He pit.

In a crystal with a homogeneous distribution of radionuclides, e.g. an ideal crystal without zonation, each emission location produces the same number of alpha particles throughout the passage of time. However, the contribution of each emitter to the concentration of He within the He pit depends on the

https://doi.org/10.5194/egusphere-2026-2590
Preprint. Discussion started: 27 May 2026

probability to implant alpha particles into the He pit. This probability is a function of the geometry of the He pit and the emitters position relative to it, as described above. In the context of in-situ (U-Th)/He dating, this emitter may or may not be located within the volume probed by the ICP pit. Consequently, an ICP pit unites emitters with vastly different contributions to the helium budget of the He pit. In contrast, each emitter contributes equally to the parent isotope concentration quantified within the ICP pit. It follows that parent and daughter isotopes measured during in-situ (U-Th)/He dating are not strictly representative of each other. This, hence, introduces an imbalance to the radiometric system. Therefore, in order to make a meaningful use of in-situ (U-Th)/He dates, the misrepresentation between the measured parent and daughter isotopes needs to be quantified.

For calculation purposes, the ICP pit can be arbitrarily subdivided into a number of hollow cylinders (referred to as "shells", see Fig. 2a) with a constant thickness, so that the radius of the ICP pit is:

$$r_{ICP} = n\Delta r \quad (1)$$

where n is the count of hollow cylinders or shells, and
Δr is their constant thickness (see also Table 1).

Each shell has an average probability to produce alpha particles that are trapped inside the He pit. However, the total number of alpha particles ejected from a shell into the He pit depends on the number of ejections from each emitter, the average concentration of emitters within the shell, and the shell's volume.

$$\alpha_{He\ pit,S} = p_\alpha * i * c_{emit} V_s \quad (2)$$

Where $\alpha_{He\ pit,S}$ is the total number of alpha particles implanted into the He pit from a specific shell,
p_α is the average probability of this shell to implant an alpha particle into the He pit,
i is the number of ejections from each emitter,
c_{emit} is the average concentration of emitters in the shell, and
V_S is the shell's volume.

Hence, each ICP pit shell's contribution to the helium budget within the He pit is:

$$ICP_{He,S}(d) = \frac{\alpha_{He\ pit,S}}{\alpha_{He\ pit,total}} = \frac{i*c_{emit}V(r)_S}{\sum_{n=0}^{n} p_\alpha * i * c_{emit} V(d_n)_S}, \quad (3)$$

Where $\alpha_{He\ pit,total}$ is the total number of alpha particles produced by a shell, and
d is the radial distance of the shell from the centre of the He pit, which relates to Δr and n as:

$$d = n\Delta r \quad (4)$$

Likewise, the contribution of each shell to the parent isotope-budget can be quantified. This is given by the emitter concentration and volume of each shell divided by the total number of parent nuclei within the ICP pit:

$$ICP_{Parent,S} = \frac{c_{emit}*V_S}{c_{emit}*V_{ICP\ pit}} = \frac{c_{emit}*\pi h*(r_1+\Delta r)^2 - r_1^2}{c_{emit}*\pi h*r_{ICP}^2} \quad (5)$$

where h is the depth of the ICP pit,
r_1 the inner radius of a shell, and
r_{ICP} the maximum radius of the ICP pit.
In a crystal with homogeneous parent isotope distribution this term simplifies to

$$ICP_{Parent,S} = \frac{2r_1+\Delta r}{n^2 \Delta r}, \quad (6)$$

https://doi.org/10.5194/egusphere-2026-2590
Preprint. Discussion started: 27 May 2026

starting at zero for the initial r_1. Having determined these two contributions, the difference between ICP_{He} and ICP_{Parent} quantifies the misrepresentation between the measured parent and daughter isotopes. However, while the calculation of ICP_{Parent} is straightforward, the calculation of ICP_{He} is not, as it depends on p_α of each shell, which is a function of the individual discrete alpha stopping distances in all relevant decay chains, the geometry of the He pit, and the radius of the shell (Figs. 2 and 3). Thus, we have developed a software, OptiPit, to calculate the probability of each shell to implant alpha particles into the He pit, p_α, from the dimensions of the He and ICP pits and the alpha stopping distances of interest, which consequently enables the quantification of the imbalance introduced to in-situ (U-Th)/He dating by the geometries of the ablated laser pits.

Table 1: Abbreviations used in the equations and throughout the text.

Symbol	Description
r_{ICP}	Maximum radius of the ICP pit
N	Number shells within the ICP pit
Δr	Thickness of the ICP pit shells [µm]
$\alpha_{He\ pit,S}$	Count alpha particles implanted into the He pit by a shell
$\alpha_{He\ pit,total}$	Count of alpha particles within the He pit
p_α	Probability of an alpha particle to be implanted into the He pit [%]
I	Number of ejections per emitter
c_{emit}	Emitter concentration [mol µm^{-1}]
V_S	Volume of a shell of the ICP pit [µm^3]
D	Radial distance of a shell from the centre of the He pit [µm]
ICP_{He}	Contribution of the ICP pit to the helium budget [%]
ICP_{Parent}	Contribution of the ICP pit to the radionuclide (parent nuclide) budget [%]
γ	Proportion of helium-generating parent ablated by the ICP pit [%]

2.2 Goal and functionality of the OptiPit software

OptiPit is an open-source software for PC written in C++20, OpenGL 4.3, and Nuklear single header GUI library, which simulates and three-dimensionally visualizes the helium redistribution by alpha ejection of ^{238}U, ^{235}U, and ^{232}Th in apatite, zircon, and titanite. Diffusion processes and radioactive lattice damage are not considered by OptiPit, but the framework allows their integration in the future. Any other mineral of interest can be added to the model as well, provided that its discrete alpha stopping distances are given by the user. OptiPit approximates the mineral as a finite cuboid cloud of evenly spaced alpha-emitting and alpha-receiving sites at a customizable density. From each site of emission, a given number of alpha particles is ejected into random directions according to the customizable concentration of U and Th, the number of alpha decays of each decay chain, and the selection between discrete or average stopping distances. Each ejection path and stopping location is then tracked by the program. Additionally, the number of alpha particles implanted into the He pit is analysed geometrically by checking if the stopping location of the particles lies within the cylinder approximating the He pit.

OptiPit has been developed focussing on the graphical output of the results. The software displays three perpendicular cross sections through the cuboid of the simulated mineral, which can be moved freely

https://doi.org/10.5194/egusphere-2026-2590
Preprint. Discussion started: 27 May 2026

through the simulation space. These cross sections show heat maps of the values held by each emission or receiver site, which can display the radionuclide concentration, the helium concentration, the number of ejections per emission site, and the probability of helium trapped p_α (see Fig. 4). Non-homogeneous radionuclide distributions, simulating crystal zonation, can be created by the user with the customization tool provided within OptiPit. This tool enables the user to create regions of customizable size and radionuclide concentration by re-sizable cubical or planar boxes for which the radionuclide concentrations can be determined individually. This zonation will thus result in a simulation with a heterogenous production of He.

Table 2: Shell-based parameters (see Figs. 2 and 3, hollow cylinders of different radii) used for simulation evaluation within OptiPit and their equations.

Shell-based results and their dependence on pit size	
Probability of helium trapped	$p_{\alpha,S}$
The mean probability of an ICP pit-shell (Fig. 2) to implant alpha particles into the He pit. $\alpha_{total,S}$ is the total number of alpha emissions from a shell. $\alpha_{He\ pit,S}$ is the number of these emissions that are implanted into the He pit. $$p_{\alpha,S} = \frac{\alpha_{He-pit,S}}{\alpha_{total,S}} = \frac{p_\alpha * i * c_{emit} V_S}{i * c_{emit} V_S} \quad (7)$$	
Number of productive parents per shell	$k_{Prod,S}$
Absolute number of productive parent nuclei in the current shell, with k_S denoting the number of emission sites of a shell. It is equal to the number of alpha particles implanted into the He pit by each shell divided by *i, the* number of ejections from each emitter. $$k_{Prod,S} = \bar{c}_{emit,S} * k_S * p_{\alpha,S} \quad (8)$$	
Contribution of a shell to the helium budget	ICP_{He}
This value is **not** exported by OptiPit and derives itself from $k_{Prod,S}$ as: $$ICP_{He,S} = \frac{k_{Prod,S}}{\sum_{S=0}^{S} k_{Prod,S}} \quad (9)$$	

Three output tables are exported by OptiPit as *.csv*-files. Two present cross-sections of the probability of helium trapped p_α and the total number of alpha particles implanted into the He pit from each emission site in the XZ-plane at *y = 0*, defined below (Fig. 4). The third output file stores the evaluation of the probability and productivity of the material within the ICP pit, along with the boundary conditions of each simulation (i.e., the size of the model in micron, the dimensions of the He pit, etc.). The evaluation of the results considers an ICP pit with either a fixed depth or a fixed radius-depth ratio. Both are evaluated from the centre of the He pit to the boundaries of the simulated cuboid.

The output values produced for a fixed depth can be divided into two groups: the first group includes two parameters calculated from the average of a shell of the current radius, e.g. a hollow cylinder of

https://doi.org/10.5194/egusphere-2026-2590
Preprint. Discussion started: 27 May 2026

finite thickness (Figs. 2 & 3), specified in Table 2. The second group includes three parameters calculated from the average of progressively larger solid cylinders specified in Table 3.

2.3 Quantification of the age offset inherent to in-situ (U-Th)/He dating

The output calculated by OptiPit allows for the quantification of the age bias inherent to in-situ (U-Th)/He dating induced by the imbalance in the quantification of He and radionuclides (Sect. 2.1) for any combination of He and ICP pit geometries. This imbalance between the measured radiogenic helium and the measured radioactive parent nuclei within the ICP pit, which depends on its radius, is calculated as the absolute difference between the contribution of all shells within an ICP pit of a specific radius to the helium budget and to the budget of radioactive nuclei:

$$mismatch = \sum_{n=0}^{n} \left| \left(ICP_{He,S} - ICP_{Parent,S} \right) \right| \quad (13)$$

where $ICP_{He,S}$ is the contribution of a shell of the ICP pit to the helium budget and $ICP_{Parent,S}$ is the contribution of a shell of the ICP pit to the radionuclide budget.

Table 3: Equations used to calculate the cylinder-based (see Fig. 3) evaluation within OptiPit.

Cylinder-based results and their dependence on pit size	
Uranium/ Thorium ICP pit	$c_{U\|Th}$
Average uranium and thorium concentration within an ICP pit (fmol * µm^{-3}), with k denoting the number of emission sites within the ICP pit and $c_{U\|Th,k}$ the U or Th concentration of each emission site (fmol * µm^{-3}). $$c_{U\|Th} = \frac{\sum_{n=0}^{n} c_{U\|Th,k}}{k} \quad (10)$$	
Proportion of helium-generating parents	γ
Proportion of all helium-generating parents captured within the volume of the ICP pit, with $k_{Prod,total}$ denoting the total number of productive emitters. $$\gamma = \frac{\sum_{S=0}^{S} k_{Prod,S}}{k_{Prod,total}} \quad (11)$$	
Productivity of parents	P
Average productivity of all parent nuclei within the ICP pit, with n_{ICP} denoting the total number of ICP pit shells. $$P = \frac{\sum_{S=0}^{S} i * c_{emit,S} * k_S * p_{\alpha,S}}{n_{ICP}} \quad (12)$$	

Following this, the calculated values for p_α and γ, as well as the chosen radius and depth of the He pit and ICP pit of a simulation run, are inserted into an Excel spreadsheet given in the supplementary material. The spreadsheet not only quantifies the mismatch in a two-dimensional simplification of the modelling done in OptiPit, but also enables a quick estimation of the age offset associated with the *mismatch*, which can be related to information about radionuclide zonation gained from BSE, cathodoluminescence, or Raman mapping, without the need of specifying the exact three-dimensional radionuclide distribution and simulating complete models within OptiPit.

https://doi.org/10.5194/egusphere-2026-2590
Preprint. Discussion started: 27 May 2026

The contribution of each shell to the helium budget $ICP_{He,S}$ is calculated from p_α, its volume, and c_{emit} as demonstrated in Eq. (3). The contribution of each shell to the budget of radioactive nuclei within the ICP pit $ICP_{Parent,S}$ is calculated following Eq. (6). Importantly, if a shell lies outside of the maximum radius of the ICP pit, its contribution to the budget of radioactive nuclei is zero, as its radionuclides are not quantified analytically, but it might still contribute to the helium budget. Because the spreadsheet determines the *mismatch* for different dimensions of the He and ICP pits, it enables an optimization of the ICP pit geometry by testing different dimensions to calculate the smallest summed *mismatch* between the contributions of each shell towards the budgets of helium and radioactive nuclei. A visual representation of this process is presented in the Result section, when we test the method to common (U-Th)/He in-situ spot geometries.

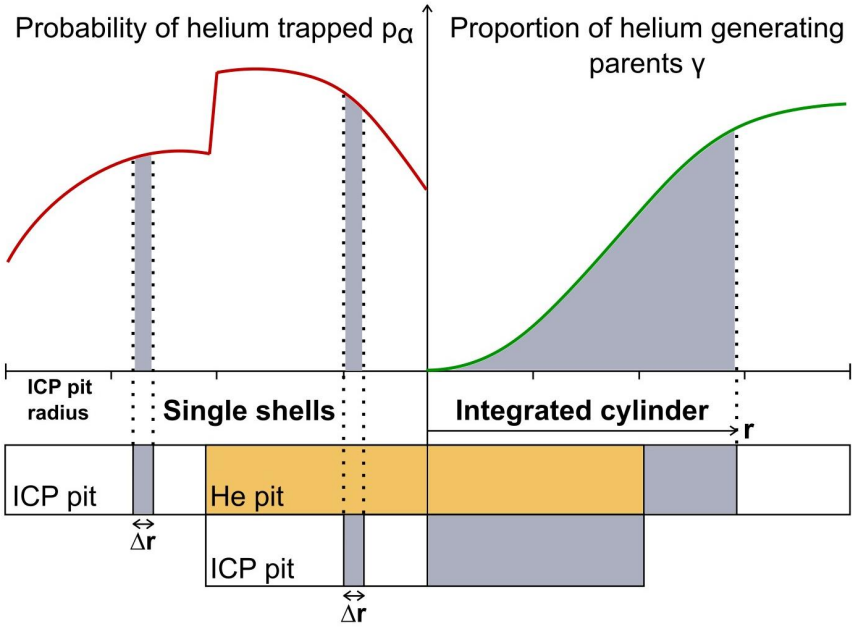

Figure 3: Sketch illustrating how shell-based (left) and cylinder-based (right) evaluations of the results produced by OptiPit are calculated. Shell-based values are calculated from the volume of one shell of the ICP pit, e.g. a hollow cylinder of specified thickness. Cylinder-based values are integrated over the volume of a solid cylinder from the centre of the ICP pit to radius r. For more information see Table 2 and 2.

Any given spot geometry is evaluated within an Excel sheet provided in the supplements. This sheet facilitates a quick calculation of both the *mismatch* and the He age offset, provided the probability of helium trapped and the proportion of helium-generating parents (*γ,* defined above; both exported from OptiPit) are copied over for all three decay chains. Thereby, lengthy calculation runs within OptiPit are avoided when the age offset of different bodies of radionuclide zonation is calculated (see section 3.4). This value is used to extrapolate the amount of He in the budget with non-quantifiable parent nuclei, corresponding to radionuclides lost during polishing into the grain and during ablation of the volume used for He extraction (referred to as “blind effect” by Léger et al. 2023). It is furthermore important

https://doi.org/10.5194/egusphere-2026-2590
Preprint. Discussion started: 27 May 2026

because the probed proportion of helium-generating parents appraises the robustness of a measurement against the implantation of He by non-analysed radionuclides. In a heterogeneous crystal, an ICP pit that captures most of the parent nuclei of the radiogenic helium in its associated He pit produces a more robust result than one that analyses only a small fraction of them. This variable is independent from *mismatch*, as an ICP pit with low *mismatch* can have a very high proportion of unconsidered productive parent nuclei and vice versa (see below, in Results). Thus, both values need to be considered to assess the quality of the geometries chosen for the laser ablation pits of in-situ (U-Th)/He dating.

Table 4: Dimensions of the two illustrative in-situ pit geometries used for pit size optimization.

Geometry	He pit dimensions [µm]			ICP pit dimensions [µm]			Examples of application
	Diameter	*Depth*	*Ratio*	*Diameter*	*Depth*	*Ratio*	
A	60	1-2	30-60	40	20	2	Evans et al. (2015)
B	25	10	2.5	65	20	3.25	Horne et al. (2016)

3. Results

The customizable nature of OptiPit allows the simulation of the alpha distribution for any laser ablation pit dimension and crystal characteristic. In this study, we focus on demonstrating that quantifiable differences exist in the results of varying laser ablation spot geometries currently used for in-situ (U-Th)/He dating. Hence, the following chapter compares the pit geometries used by two schools of thought which are common in in-situ (U-Th)/He dating (Fig. 4, Table 4). The first (Geometry A), exemplified by Evans et al. (2015), combines very wide (diameter about 60 µm) and shallow (<1-2 µm deep) He pits with narrower but much deeper ICP pits (Fig. 4(A)). Another example of combining a wide He pit with a narrower and deeper ICP pit is Vermeesch et al. (2012). Contrary, Geometry B is exemplified by Horne et al. (2016) and combines a narrower but deeper He pit (diameter about 25 µm, depth about 10 µm) with a much wider and similar or deeper ICP pit, aiming to capture the whole available volume that can implant helium into the He pit (Fig. 4(B)). Similar dimensions were used by Léger et al. (2023), and Dunkl et al. (2024).

3.1 Alpha redistribution modelling

Modelling of the illustrative He pit geometries (Table 4), considering zircon as the analysed mineral, reveals where the helium analysed by each of them will have been produced. As the pit geometries investigated by OptiPit are radially symmetric, the distribution of p_α in three dimensions can be expressed by cross-sections parallel to the z-axis of the simulation transversing the centre of the He pit (Fig. 4). Evidently, the probability of helium to be trapped in a very shallow He pit (Geometry A) is generally much smaller than for the narrower but deeper He pit (Geometry B), because the smaller dimension of the He pit limits the largest possible intersection area between the He pit and the alpha

https://doi.org/10.5194/egusphere-2026-2590
Preprint. Discussion started: 27 May 2026

ejection spheres (Figs. 2, 4(A)). The values of p_α within the shells of the ICP pit, i.e., the average probabilities of each shell, are shown in Fig. 5a. They exemplify that, for both approaches, the material ablated by the ICP pit represents the average p_α around the He pit, even though only a sub-volume of the total productive volume is probed.

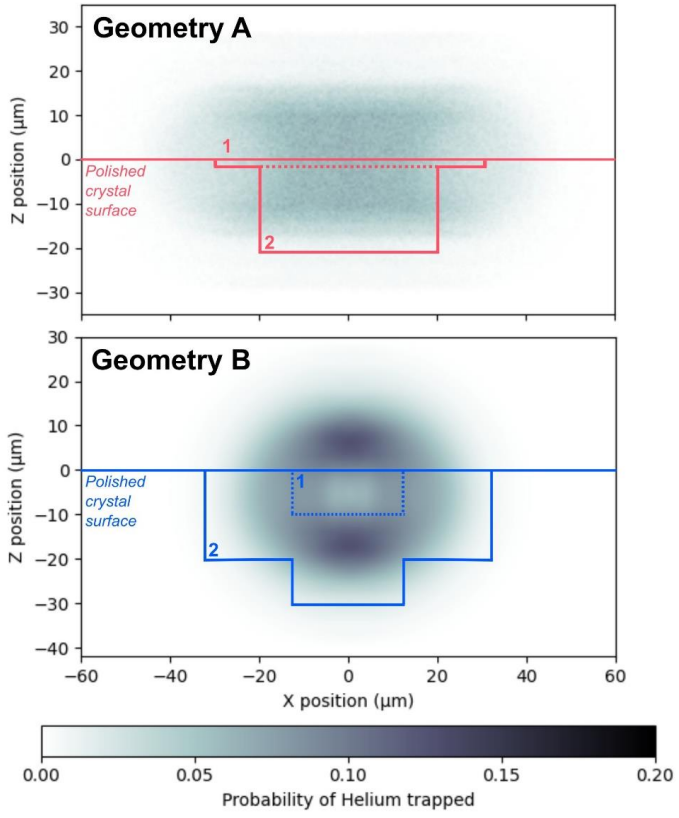

Figure 4: Heatmaps showing the position of the He-generating atoms and their probability to implant radiogenic helium in the He-pit as a cross section through the laser ablation spots. Homogeneity and 1:1 Th/U ratio are assumed for the calculation.

Furthermore, the volume effectively implanting helium into the He pit is larger for the wide He pit (Fig. 4(A)). This fact, together with the generally lower p_α calculated for Geometry A, are reflected in the portion with which each shell impacts the number of productive parent nuclei, $k_{prod,S}$, which is equal to the share of each shell in the helium budget (Fig. 5b). Considering Geometry A, the shallow He pit combined with a narrow but deep ICP pit analyses less of the material that effectively contributes to the helium budget compared to Geometry B, which is evident from the proportion in helium-generating parents quantified by each combination of spot geometries (Figs. 4, 5c). Additionally, the wide He pit has a lower maximum proportion of helium-generating parents that could potentially be quantified by

https://doi.org/10.5194/egusphere-2026-2590
Preprint. Discussion started: 27 May 2026

the LA-ICP-MS analysis using the biggest possible pit size compared to the deep He pit (47% compared to 52%, Fig. 5c).

Lastly, a comparison between the contribution of each shell to the helium budget (ICP_{He}) and the radionuclide budget (ICP_{Parent}) is shown in Fig. 5d. Geometry A results in a high overrepresentation of all shells within the ICP pit in the radionuclide budget (Fig. 5d, dashed red line) compared to their contribution to the helium budget (solid red line), which corresponds to an imbalance between both sides of the geochronometer. This geometry furthermore only incorporates about a third of the parent nuclei available for dating into the measurement (Fig. 5c). Contrary to that, Geometry B underestimates ICP_{Parent} in all shells with a radius smaller than 23 µm compared to ICP_{He} (Fig. 5d, blue lines), whereas the opposite is true for shells with larger radii, while analysing 96% of the radionuclide available for analysis (Fig. 5c). The higher proportion in helium-generating parents on its own suggests that Geometry B is more appropriate for in-situ (U-Th)/He dating.

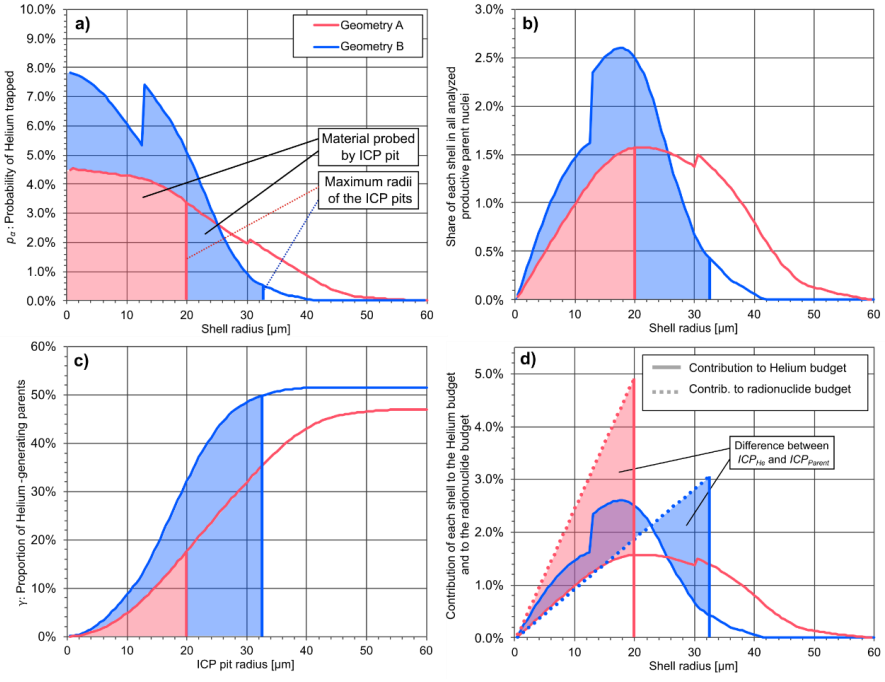

Figure 5: ICP pit-radius-dependent functions of the parameters calculated by OptiPit for the two geometries depicted in Fig. 4 (details in Table 4). The radius of the ICP pits considered by these geometries is accentuated as vertical lines in each graph. a) Probability of helium trapped $p_{\alpha,S}$, b) Share of productive parent nuclei $k_{Prod,S}$ = $ICP_{He,S}$, c) Proportion of helium-generating parents γ, and d) comparison of ICP_{He} and ICP_{Parent}. Homogeneity and 1:1 Th/U ratio are assumed for the calculation.

https://doi.org/10.5194/egusphere-2026-2590
Preprint. Discussion started: 27 May 2026

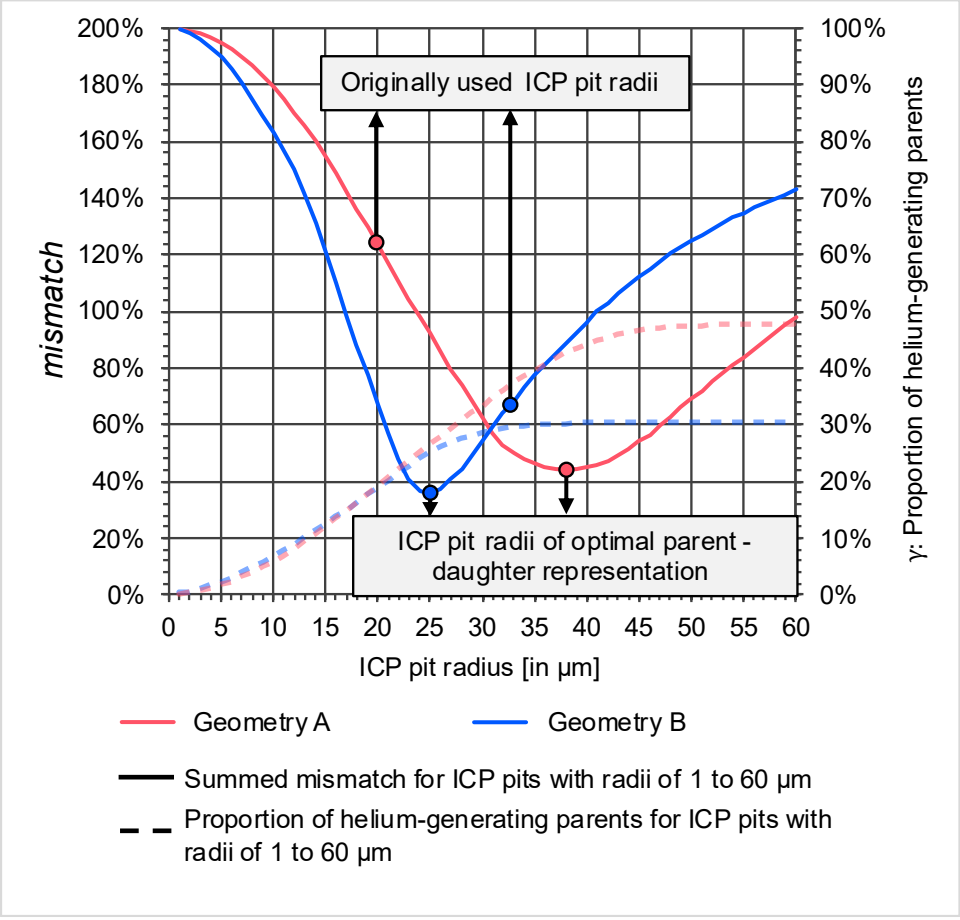

Figure 6: Sum of the absolute mismatch *for both discussed laser ablation pit geometries for different ICP pit radii. The optimal radii, e.g. those with the smallest summed difference between* ICP_{He} *and* ICP_{Parent} *are marked with vertical lines. Homogeneity and 1:1 Th/U ratio are assumed for the calculation.*

3.2 Parent-daughter imbalance quantification

Figure 5d exemplifies the parent-daughter imbalance inherent to in-situ (U-Th)/He dating, resulting from the difference in the relative contribution of the shells of the ICP pit to the helium and radionuclide budgets, as well as the opportunity for optimization. Whereas ICP_{Parent} increases linearly with the volume of each shell, ICP_{He} is a complex function which depends on the dimensions of the He pit and the depth of the ICP pit. This function intercepts the origin and decreases to zero at radii higher than the radius of the He pit plus the longest alpha stopping distance. Between these, the curve experiences at least one maximum but may experience more local maxima and minima. The result is that the sum of the local differences of ICP_{Parent} and ICP_{He}, (i.e., *mismatch*, eq. 13) can never be zero. However, *mismatch* can be minimized by optimizing the radius of the ICP pit, which changes the slope of ICP_{Parent} and increases the agreement between the contribution of each shell to the helium and radionuclide budgets.

https://doi.org/10.5194/egusphere-2026-2590
Preprint. Discussion started: 27 May 2026

The $mismatch$ curves calculated as a function of the radius of the ICP pit for the two geometries are presented in Fig. 6a, together with the proportion of helium-generating parents that is ablated by each ICP pit radius. In this diagram, the radius for which mismatch reaches its minimum (44.4% and 35.6%, respectively) corresponds to the ideal ICP spot size which enables dating of the (U-Th)/He closest to equilibrium – these are about 38 µm for Geometry A and 25 µm for Geometry B, compared to the originally used 20 and 28 µm, respectively. Both optimized ICP pits analyse material beneath and around the He pit, instead of only analysing material beneath it as in the approach followed by Evans et al. (2015). Despite the optimization of the ideal ICP radii determined from Fig. 6, a zero *mismatch* is inevitable for the entire ICP pit. Some shells will always be overrepresented in the helium budget compared to the radionuclide budget and vice versa, and each combination of pits will result in a particular mismatch profile (Fig. 7). This has implications for (U-Th)/He date calculations if the analysed crystal volume is not homogeneous (see below). However, the sum of the absolute *mismatch* values of all shells is lowest for the optimized geometries (dashed curves) and considerably lower than for the original geometries (dashed curves in Fig. 7).

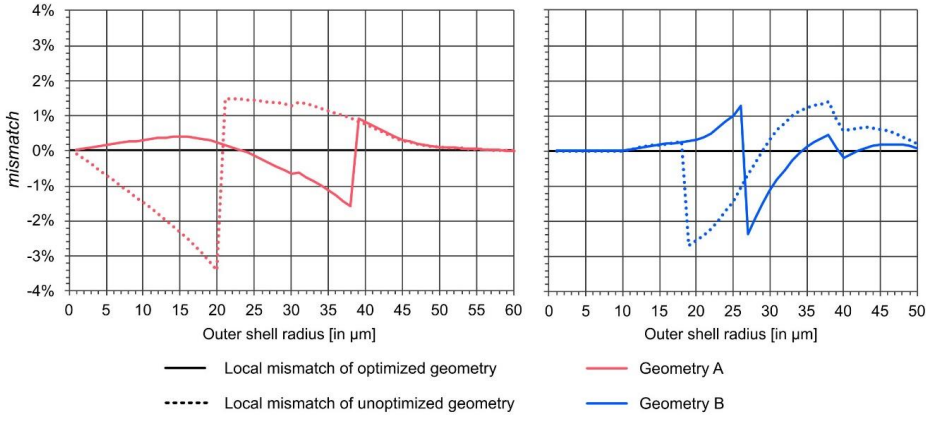

Figure 7: Comparison of the mismatch of each ICP pit shell between the original and optimal versions of two illustrative geometries (Table 2).

3.3 Importance for the in-situ (U-Th)/He age

Because *mismatch* describes the analytical imbalance inherent to in-situ (U-Th)/He dating, it can also express the age offset introduced to the apparent age if radionuclide zonation produces an excess or lack of alpha particles implanted into the He pit relative to a homogeneous crystal volume. It captures how radionuclide zonation within any shell of the ICP pit produces He age estimates that significantly exceed or fall short of the true He age. As we define *mismatch* as the contribution of a shell to the helium budget subtracted by its contribution to the radionuclide budget, positive values mean that a given shell has a bigger share in the measured helium concentration than it has in the radionuclide concentration. This means that an elevated radionuclide concentration in these shells increases the helium concentration in the pit more strongly than the measured average radionuclide concentration in the ICP pit, and thus the (U-Th)/He age will be overestimated. Conversely, a lower radionuclide

https://doi.org/10.5194/egusphere-2026-2590
Preprint. Discussion started: 27 May 2026

concentration in this shell results in an underestimation of the He age. The opposite is true for shells with a negative *mismatch* value, as these shells impact the helium budget less than the radionuclide budget.

3.4 Modelling the impact of zonation and pit geometry on the He age bias

By using the mismatch quantification described above, the offset of any in-situ (U-Th)/He date can be estimated for different crystal zoning patterns. The most easily available data for this two-dimensional visualization of zonation are the frequently used cathodoluminescence and BSE images, or Raman spectroscopy maps of polished grains. One can assume that they are representative of the complex three-dimensional zonation of the natural crystal. In order to illustrate the impact of a chosen pit geometry in He age dispersion in such a situation, we carried out calculations for the exemplified in-situ geometries, considering the original and the optimized ICP pit radii for both pit geometries (Fig. 7). Two different cases of tabular radionuclide zonation in the vicinity of the He pit have been modelled. Firstly, a tabular zone oriented parallel to the incident laser beams with a fivefold radionuclide concentration is moved into the volume probed by the in-situ pits from the outside, until it encompasses half of the in-situ pits (Fig. 8). This geometry mimics the common situation when the in-situ pit is placed in an elongated zircon that has c-parallel actinide zonation along the prismatic crystal faces. The opposite situation is modelled by simulating a narrow tabular zone located in the centre of the ablation spots and increasing its thickness until it reaches the border of the ICP pit and encompasses on half of the in-situ pits (Fig. 9).

In the first case, as the rectangle of increased radionuclide zonation is moved into the in-situ pits with Geometry A, any zonation that lies outside of the radius of the narrow ICP pit produces an overestimation of the He age (Fig. 8a). This is evident, as any radionuclides located between the outer edge of the ICP pit but still within the volume that can implant helium into the He pit (Fig. 4) contribute to the He budget, but not for the radionuclide budget (Fig. 5d). This effect increases as the zonation approaches the border of the ICP pit, where the probability to implant helium into the He pit increases, while the representation in the radioactive budget remains zero. The maximum He age offset produced in this scenario is an overestimation of the age by 63%. Once the zonation border crosses this maximum, any radionuclide budget inside of the ICP pit is strongly overrepresented compared to the

https://doi.org/10.5194/egusphere-2026-2590
Preprint. Discussion started: 27 May 2026

helium budget. This reduces the age offset progressively to zero, which is achieved when the zonation covers half of the ICP pit, at which point the impact of the zonation is nullified.

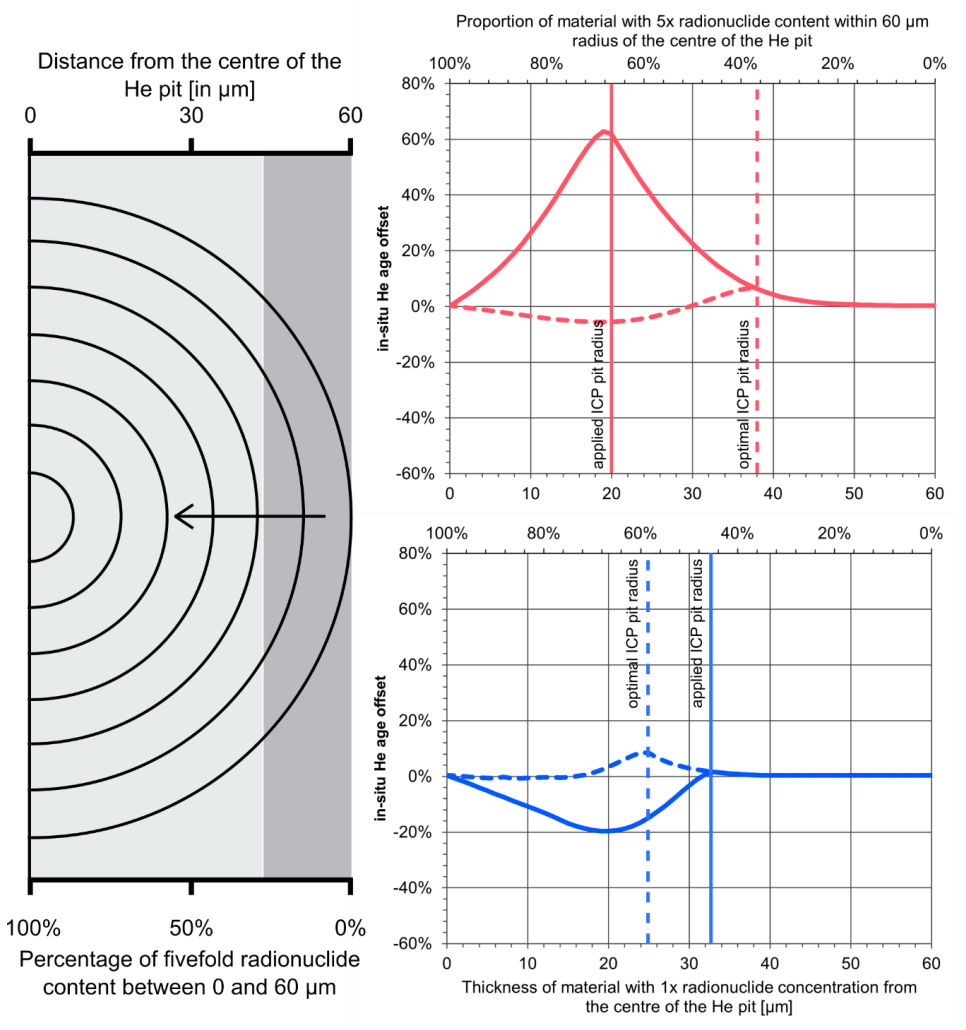

Figure 8: He age offset calculated for the optimized ICP pit radii (dashed lines) and the originally used ICP pit radii (Table 4, solid lines), induced by progressively moving a fivefold radionuclide zonation into the in-situ pits. Geometry A is shown in the top, Geometry B in the bottom.

In the second scenario, the volume of increased radionuclide zonation increases in size from the centre of the He pit and gradually encompasses one of its halves, meaning that the area of smaller actinide concentration is pushed out of the pits. In this case, the offset of the He age for Geometry A behaves in the opposite way to that of the previous example (compare Figs. 8 and 9). Thus, the relative overestimation of radionuclides compared to helium produces an increasing underestimation of the (U-Th)/He age until the outer rim of the ICP pit is reached (Fig. 9a). Only beyond this point does the representation of additional radionuclides reach zero, so that the radiogenic helium produced by this

https://doi.org/10.5194/egusphere-2026-2590
Preprint. Discussion started: 27 May 2026

415 portion of the crystal is strongly overestimated, reducing the age offset until, again, it reduces to zero as one half of the in-situ pits is completely encroached by the radionuclide zonation. The maximum age offset reached for this kind of zonation is -23%, again reached when the border of the zonation is located right at the boundary of the ICP pit.

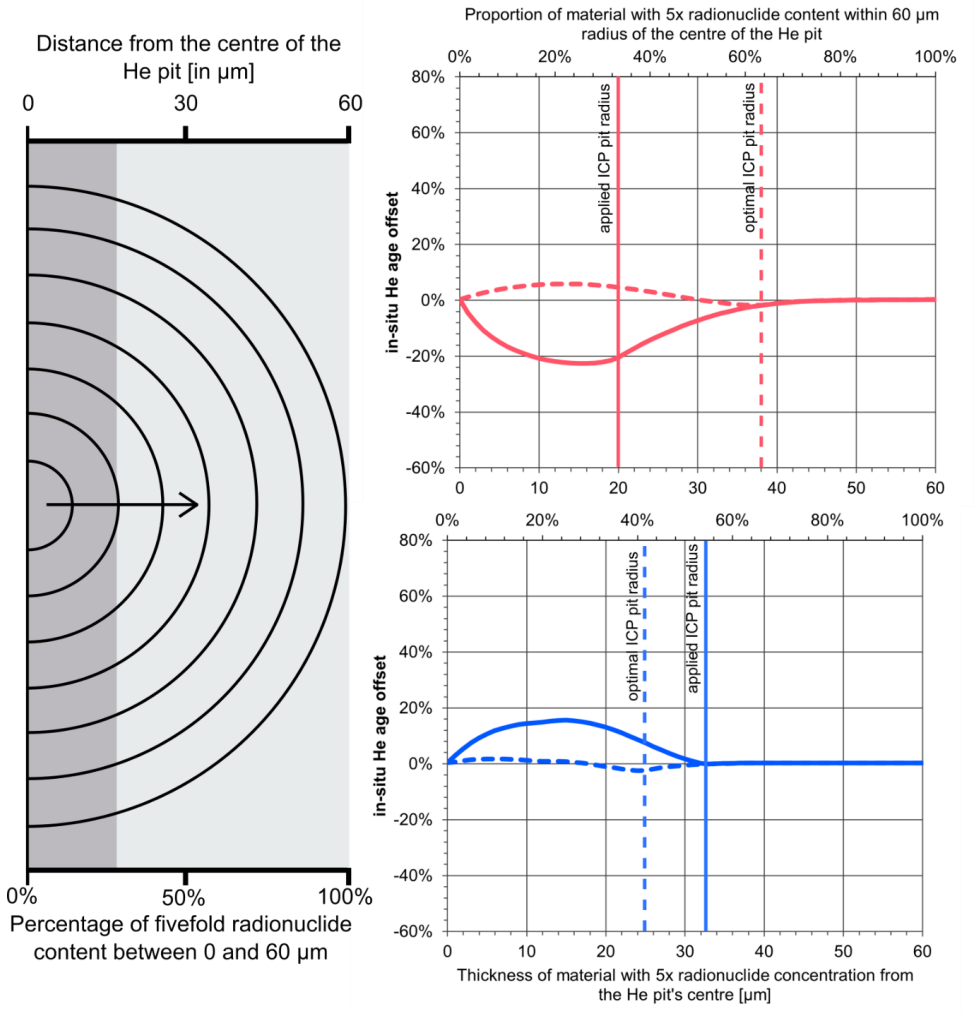

420 *Figure 9: He age offset calculated for the optimized ICP pit radii (dashed lines) and the originally used ICP pit radii (Table 4, solid lines), induced by a fivefold radionuclide zonation which progressively grows from within the in-situ pits to the rim of the ICP pit. Geometry A is shown in the top, Geometry B in the bottom.*

Conversely, Geometry B, in which a deep He pit is combined with a wider and deeper ICP pit, is also
425 subject to the age offsets due to *mismatch*, but its impact in the resulting He ages is the opposite to that of Geometry A. The radionuclides beyond about 23 µm from the centre of the He pit are strongly overrepresented compared to their radiogenic daughters inside of the He pit. The reason for this is that this geometry strives to integrate most of the radioactive parents which could have contributed to the

https://doi.org/10.5194/egusphere-2026-2590
Preprint. Discussion started: 27 May 2026

helium budget of their in-situ pits (Fig. 5d). However, any radioactive material within 23 µm has a very high probability of producing helium that will contribute to the He pit and is therefore strongly underrepresented in the radionuclide budget (Fig. 5d). Thus, as the ICP pit is encroached by a zone with elevated radionuclide concentration, its age estimate is increasingly too low, reaching a maximum offset of -20% for a fivefold zonation beyond about 20 µm (Fig. 8b). Conversely, if the zonation occupies the ICP pit from the middle of the in-situ pits, the age is increasingly overestimated until the boundary of the zonation reaches about 13 µm from the centre of the He pit, resulting in a maximum offset of 16% (Fig. 9b). Beyond this distance, the offset falls back to zero until the radionuclide zonation occupies half of the in-situ pits.

Importantly, the in-situ (U-Th)/He age offset is strongly reduced both for Geometry A and Geometry B if the optimal ICP pit geometries are used (Figs. 8 and 9, dashed lines). While the offset still depends on the location of the zonation boundary and its corresponding *mismatch*, its value is minimized, which minimizes the He age offset as well. Instead of producing over- or underestimations of +63% and -23% for in-situ pits following Geometry A, the maximum He age offset can be reduced to a range of +7% to -6% for both zonation types. Likewise, the He age offset of Geometry B is reduced from a maximum of -20% and +16% to a range of +8% to -1% for radionuclide zonation enveloping the pits from the outside and +2% to -2% for the zonation growing from the inside. Thus, our model demonstrates that an optimization of the He pit geometry is possible and has the power to produce significantly less dispersed in-situ (U-Th)/He ages.

4. Discussion – Implications for in-situ pit geometries

Modelling of the *mismatch*-related age offset of in-situ (U-Th)/He dating demonstrates that this technique does not fulfil the condition of equilibrium required for calculating radiometric ages as soon as the analysed material is not perfectly homogeneous. This remains true for any measurement done by this method, as the method's destructive nature forbids the measurement of all radioactive parent isotopes from which the analysed radiogenic He is derived. Furthermore, the influence of all shells on the helium budget and on the radionuclide budget cannot simply be brought into complete agreement without using exceedingly complex ICP pit geometries which mimic the complex radius-dependent trend of $ICP_{He,S}$ in $ICP_{Parent,S}$. Thus, the *mismatch* remains always greater than zero, always subverting the basic assumption of measuring related and comparable parent and daughter nuclei.

However, the optimization of the geometries of the in-situ pits provides a theoretical foundation for estimating the uncertainties of the method to a higher degree of confidence. Firstly, the modelling demonstrates that a simple radionuclide zonation which homogeneously envelops one half of the material probed by the laser ablation spots does not have an impact on the in-situ age if diffusion and radioactive damage are disregarded. This statement can be broadened so that any homogeneous zone which completely envelops a sector of a circle centred around the He pit does not influence the He age produced by the measurement, independent of its relative radionuclide enrichment or depletion. Thus, this suggests that the dating of given spots within a crystal which have radionuclide zonation with

https://doi.org/10.5194/egusphere-2026-2590
Preprint. Discussion started: 27 May 2026

favourable geometry may be viable even in strongly zoned crystals if the location of the in-situ pits relative to the zonation is chosen correctly.

Furthermore, *mismatch* develops from the centre of the He pit outwards as a function of *r*, depending on the radius of the ICP pit. This function may reach zero or values close to zero for some shells of the ICP pit with specific radii (Fig. 7). Any radionuclide zonation located at sites with such a small or non-existent mismatch does not produce a bias in the He age, as their contribution to the helium and radionuclide budgets is balanced. Thus, laser ablation pits can theoretically be placed in regions of near-punctual radionuclide variation, (e.g., uraninite or thorite inclusions in zircon) without these anomalies influencing the He age significantly.

However, in-situ (U-Th)/He dating zircon grains which experienced high self-irradiation induces modifications of their helium retentivity and closure temperature (Guenthner et al. 2013). Radionuclide zonation of these grains often modifies these characteristics at a sub-crystal level, so that zircon grains constitute a heterogeneous medium with different alpha damage densities, helium solubilities, and hence closure temperatures (Anderson et al. 2020; Danišík et al. 2017). Consequently, if an in-situ date is measured along the border between two or more regions of different radionuclide zonation, the He age may be affected not only by intracrystalline alpha ejection, but also by diffusive He migration due to the contrast in He retentivity of the probed material. Thus, the theoretical differences in closure temperatures and their impact on the in-situ He age must always be kept in mind when interpreting in-situ ages, even if the spot geometry and location have been optimized.

Another consequence of the modelling results is that not every possible He pit can reasonably be combined with its optimized ICP pit. The optimal ICP pit radius typically exceeds the radius of its He pit, as ICP_{He} has a complex right-skewed distribution, while ICP_{Parent} is a linear function with an increasing slope for decreasing ICP pit radii (Fig. 5d). The skewness always extends beyond the border of the He pit, at which a second maximum in ICP_{He} may be developed (e.g. Fig 5b, red line). Its absolute maximum furthermore lies at, or beyond, the borders of a He pit with a radius and depth less than the most common stopping distances (about 16 to 20 µm in zircon). This position results in the maximum intersection area between the alpha ejection spheres and the He pit (Fig. 2). The match between this distribution and a linearly-increasing function like ICP_{Parent} which results in the smallest *mismatch* must, therefore, always lie beyond the maximum of ICP_{He}. Since the maximum of ICP_{He} lies close to the borders of the He pit for most geometries, an optimized ICP radius always results in overprinting the He pit with a larger ICP pit, if the He age offset produced by radionuclide zonation is to be minimized.

Admittedly, the applicable maximum spot size for in-situ (U-Th)/He dating is limited by the size of the available grain, the dimensions of its diffusion domain(-s), and the scale and extent at which radionuclide zonation is present. While the effects of simple radionuclide zonation can be minimized by using an optimal pit geometry, complex radionuclide zonation cannot be avoided by this optimization. Furthermore, the availability of appropriate grain sizes (or its diffusion domains) for wide He pits is limited. This makes wide He pits hardly applicable to many samples, as the domain size necessary to drill a laser ablation spot as big as 80 µm in diameter may not be available, which would be required for Geometry A. He pits of smaller diameter and higher depth, however, combined with an optimally sized ICP pit, can be applied with much more versatility.

https://doi.org/10.5194/egusphere-2026-2590
Preprint. Discussion started: 27 May 2026

Furthermore, the analytical gains of increasing the depth of the He and ICP pit should always be weighed against the potential risks. Firstly, the radionuclide zonation at depth is not known. Consequently, increasing the depth of the He or ICP pit increases the probability of capturing a radionuclide zonation which may bias the He age in an unexpected way. Secondly, increasing the depth of the He pit at a given radius increases the blind effect of the helium produced by parent nuclei within the He pit. However, the consequent reduction in the proportion of helium-generating parents measurable by the ICP pit may be offset by the decrease in the fraction held by the radioactive material lost by polishing, the amount of which remains constant and independent of the depth of the He pit. In other words, increasing the depth of the He pit shifts the volume responsible for He production towards the interior of the crystal relative to the polished surface (Fig. 4). Regardless, limiting both depth and radius of the He pit limits the amount of helium released by ablation, which reduces the applicability of the method to young and radionuclide-poor samples and minerals. The assessment of these effects is subjective and varies among different samples, ultimately being left to the operator.

Léger et al. (2023) draw similar conclusions about the optimal size and geometry of in-situ (U-Th)/He laser pits. They describe that a He pit with a radius and depth of 15 µm each, combined with an ICP pit of similar depth and a radius of 30 µm, represent the optimal in-situ pit geometry. While a justification for this assessment is not given, our modelling performed using OptiPit agrees with this finding, as it produces the same optimal ICP pit radius. However, our model reveals that the higher depth of the He pit and the consequently larger volume probed compared to our optimized Geometry B (Fig. 6) produces a lower maximum value of helium-generating parents (at most 39% of all parents). In other words, the amount of helium produced by radionuclides ablated during helium quantification, to which Léger et al. (2023) refer to as “blind effect”, is higher in their set-up than for our Geometry B (in which 46% of all parent nuclei are quantified). Thus, if the analytical uncertainty allows for the extraction of a lesser quantity of helium from a sample, a He pit shallower than 15 µm should be preferred for radii of 15 µm. Furthermore, Léger et al. (2023) present in-situ (U-Th)/He ages combined with cathodoluminescence images of the dated grains, which are grouped according to the internal structure of their zonation. Their Group 6 contains 31 grains which have a lower cathodoluminescence intensity in their centre relative to their rim (which is where the in-situ pits are placed). This can relate to higher radioactive lattice damage in the centre and, consequently, an increased radionuclide concentration (Léger et al. 2023). These grains consistently overestimate the He age, yielding a higher mean age than the other groups (Léger et al. 2023). This is in accordance with the predictions of our model, as the mismatch for the central shells of the ICP pit predicts an overrepresentation of these in the helium budget for their applied pit geometry and, thus, an overestimation of the He age. Moreover, our model predicts an underestimation of the He age if the core of the He pit has a lower radionuclide concentration than its surroundings. This might be reflected by Group 1 of Léger et al. (2023) which produce a decreased mean He age, although definite conclusions cannot be drawn because of the small sample size (n = 6). Because OptiPit enables the prediction of the impact of any radionuclide zonation on the in-situ (U-Th)/He age of laser ablation pits of vastly different dimensions, we can demonstrate that in-situ pits with dimensions that deviate from the ones used by Léger et al. (2023) can produce both an under- and an overestimation of the age from the same zonation styles (compare Figs. 8 and 9). Additionally, OptiPit

https://doi.org/10.5194/egusphere-2026-2590
Preprint. Discussion started: 27 May 2026

enables any user to easily introduce arbitrarily complex three-dimensional radionuclide zonation into the alpha redistribution model and, thus, explore further scenarios. In other scenarios, it provides an estimate of the uncertainty solely caused by alpha redistribution, which may be subsequently blurred or intensified by diffusion.

Lastly, the impact of the geometry of in-situ pits and the resulting offset in the in-situ (U-Th)/He age was also predicted previously (e.g. Léger et al. 2023). However, a sound model for the distribution of genetically-related parent and daughter isotopes throughout the laser ablation pits, which establishes the link necessary for the dating of any radioactive system, has yet to be published. This is achieved by OptiPit which allows the evaluation of the parent-daughter relationship of uranium, thorium, and radiogenic He. It demonstrates that radionuclide zonation in the vicinity of the in-situ spots can both positively and negatively impact the He age depending on the size and location of the zonation as well as the dimensions of the in-situ pits. Combined with pseudo-depth profiling of uranium and thorium (Léger et al. 2023) it may enable a reliable reduction of the age bias and high age dispersion associated with in-situ (U-Th)/He dating in the future.

5. Conclusions

OptiPit demonstrates that the interplay between radionuclide zonation within crystals and the geometries of the laser ablation pits used in in-situ (U-Th)/He dating controls the age bias and dispersion inherent to the method. We furthermore demonstrate that in-situ (U-Th)/He dating cannot adequately account for the imbalance between parent and daughter isotopes in heterogeneous crystals, which is a major cause of dispersion in datasets acquired by this method. However, this effect can be mitigated depending on the information available about a grain's radionuclide zonation. If in-situ pits are shot blindly, that is without knowledge about the radionuclide zonation, the dispersion is minimized best if the ICP pit geometry is set to minimize the misrepresentation of the ICP pit in the radionuclide and helium budgets. Contrary, if data is available on the spatial distribution of mother elements, the laser ablation pits may be moved into the optimal position relative to the zonation. Lastly, we demonstrate that the reliability of any in-situ (U-Th)/He analysis can be evaluated if the dimensions of the in-situ pits are known and information about radionuclide zonation and magnitude is available for the analysed area. Thus, future studies are strongly encouraged to publish the dimensions of their in-situ pits and invest resources into acquiring compositional or structural maps of the probed areas in order to improve the quality, transparency, and comparability of the produced dataset.

Code availability

A compiled *.exe* for Windows PCs with all necessary sources and library files is available at ReSeed: https://rdms.rd.ruhr-uni-bochum.de/concern/datasets/rb68xh68k?locale=en. The C++20 source code necessary for rebuilding OptiPit from scratch is also available there.

https://doi.org/10.5194/egusphere-2026-2590
Preprint. Discussion started: 27 May 2026

Author contributions

István Dunkl conceptualized the idea. Hagen Hoemann developed OptiPit and the methodology and performed simulations and data analysis. Mathias Hueck and István Dunkl tested OptiPit. Hagen Hoemann prepared the manuscript with contributions from all co-authors.

Competing interests

The authors declare that they have no conflict of interest.

Acknowledgements

We thank Birk Härtel for the encouraging discussions on the functionalities of OptiPit and possible ways to give meaning to the created data.

Financial support

This work is supported by the German Research Council (Deutsche Forschungsgemeinschaft) under project number 542908113.

References

Anderson, A. J.; Hanchar, J. M.; Hodges, Kip V.; van Soest, M. C. (2020): Mapping radiation damage zoning in zircon using Raman spectroscopy: Implications for zircon chronology. In: *Chemical Geology* 538, pp. 119494. DOI: 10.1016/j.chemgeo.2020.119494.

Baughman, J. S.; Flowers, R. M. (2020): Mesoproterozoic burial of the Kaapvaal craton, southern Africa during Rodinia supercontinent assembly from (U-Th)/He thermochronology. In: Earth and Planetary Science Letters 531, 13 pages.

Belyaev, A.; Ross, D. (2021): The Basics of Nuclear and Particle Physics. Cham: Springer International Publishing, 401 pages.

Boyce, J. W.; Hodges, K. V.; Olszewski, W. J.; Carpenter, B. D.; Reiners, P. W. (2006): Laser microprobe (U-Th)/He geochronology. In: *Geochimica et Cosmochimica Acta* 70, pp. 3031–3039.

Brown R.W., Beucher R., Roper S., Persano C., Stuart F. and Fitzgerald P. (2013) Natural age dispersion arising from the analysis of broken crystals: Part I. Theoretical basis and implications for the apatite (U–Th)/He thermochronometer. Geochem. Cosmochim. Acta, doi:10.1016/j.gca.2013.05.041.

Danišík, M.; McInnes, B. I. A.; Kirkland, C. L.; McDonald, B. J.; Evans, N. J.; Becker, T. (2017): Seeing is believing: Visualization of He distribution in zircon and implications for thermal history reconstruction on single crystals. In: *Sci. Adv.* 3 (e1601121). DOI: 10.1126/sciadv.1601121.

https://doi.org/10.5194/egusphere-2026-2590
Preprint. Discussion started: 27 May 2026

Dobson, K. J.; Stuart, F. M.; Dempster, T. J. (2008): U and Th zonation in Fish Canyon Tuff zircons: Implications for a zircon (U–Th)/He standard. In: *Geochimica et Cosmochimica Acta* 72 (19), pp. 4745–4755. DOI: 10.1016/j.gca.2008.07.015.

Dunkl, I.; Malis, F.; Lünsdorf, N. K.; Schönig, J.; von Eynatten, H. (2024): Zircon U-Pb-He Double Dating of Modern Sands From the Inn River Catchment: Assessing Resolution and Potential in a Complex Orogenic Setting. In: JGR Earth Surface, 21 pages. DOI: 10.1029/2023JF007360.

Ehlers, T. A.; Farley, K. A. (2003): Apatite (U-Th)/He thermochronometry: methods and applications to problems in tectonic and surface processes. In: Earth and Planetary Science Letters 206, pp. 1-14.

Evans, N. J.; McInnes, B. I. A.; McDonald, B.; Danišík, M.; Becker, T.; Vermeesch, P. et al. (2015): An in situ technique for (U–Th–Sm)/He and U–Pb double dating. In: *J. Anal. At. Spectrom.* 30 (7), pp. 1636–1645. DOI: 10.1039/C5JA00085H.

Farley, K. A.; Wolf, R. A.; Silver, L. T. (1996): The effects of long alpha-stopping distances on (U-Th)/He ages. In: *Geochimica et Cosmochimica Acta* 60, pp. 4223–4229.

Farley, K. A. (2002): (U-Th)/He Dating: Techniques, Calibrations, and Applications. In: Reviews in Mineralogy and Geochemistry 47(1), pp. 819-844.

Fitzgerald, P. G.; Baldwin, S. L.; Webb, L. E.; O'Sullivan, P. B. (2006): Interpretation of (U–Th)/He single grain ages from slowly cooled crustal terranes: A case study from the Transantarctic Mountains of southern Victoria Land. In: Chemical Geology 225, pp. 91-120.

Flowers, R. M.; Zeitler, P. K.; Danišík, M.; Reiners, P. W.; Gautheron, C.; Ketcham, R. A.; Metcalf, J. R.; Stockli, D. F.; Enkelmann, E.; Brown, R. W. (2023): (U-Th)/He chronology: Part 1. Data, uncertainty, and reporting. In: GSA Bulletin 135, no. 1/2, pp. 104-136. DOI: https://doi.org/10.1130/B36266.1.

Glotzbach, C.; Ehlers, T. A. (2024): Interpreting cooling dates and histories from laser ablation in situ (U–Th–Sm)/He thermochronometry: a modelling perspective. In: *Geochronology* 6 (4), pp. 697–717. DOI: 10.5194/gchron-6-697-2024.

Guenthner, W. R.; Reiners, P. W.; Ketcham, R. A.; Nasdala, L.; Giester, G. (2013): Helium diffusion in natural zircon: Radiation damage, anisotropy, and the interpretation of zircon (U-Th)/He thermochronology. In: *American Journal of Science* 313 (3), pp. 145–198. DOI: 10.2475/03.2013.01.

Härtel, B.; Jonckheere, R.; Wauschkuhn, B.; Hofmann, M.; Frölich, S.; Ratschbacher, L. (2021): Zircon Raman dating: Age equation and calibration. In: *Chemical Geology* 579, pp. 1-8.

Horne, A.M., van Soest, M.C., Hodges, K.V., Tripathy-Lang, A., Hourigan, J.K. (2016): Integrated single crystal laser ablation U/Pb and (U–Th)/He dating of detrital accessory minerals – Proof-of-concept studies of titanites and zircons from the Fish Canyon tuff. Geochimica et Cosmochimica Acta, 178, 106-123. http://dx.doi.org/10.1016/j.gca.2015.11.044

Hourigan J. K.; Reiners, P. W.; Brandon, M. T. (2005): U-Th zonation-dependent alpha-ejection in (U-Th)/He chronometry. In: Geochimica et Cosmochimica Acta 69, no. 13, pp. 3349-3365.

https://doi.org/10.5194/egusphere-2026-2590
Preprint. Discussion started: 27 May 2026

Hueck, M.; Dunkl, I.; Heller, B.; Basei, M. A. S.; Siegesmund, S. (2018): (U-Th)/He Thermochronology and Zircon Radiation Damage in the South American Passive Margin: Thermal Overprint of the Paraná LIP?. In: Tectonics 37, pp. 4068-4085.

Jonckheere, R.; Gögen, K. (2001): A Monte-Carlo calculation of the size distribution of latent alpha-recoil tracks. In: *Nuclear Instruments and Methods in Physics Research B* 183, pp. 347–357.

Ketcham, R. A.; Gautheron, C.; Tassan-Got, L. (2011): Accounting for long alpha-particle stopping distances in (U–Th–Sm)/He geochronology: Refinement of the baseline case. In: *Geochimica et Cosmochimica Acta* 75 (24), pp. 7779–7791. DOI: 10.1016/j.gca.2011.10.011.

Léger, J.; Pik, R.; Tibari, B.; Ternois, S.; Ford, M.; Peiffert, C.; Mercadier, J. (2023): Laser Ablation (U-Th-Sm)/He Dating of Zircons: Analytical Age Bias and its Consequence for Studying Detrital Zircon Populations. In: *Geostandard Geoanalytic Res* 47 (2), pp. 219–242. DOI: 10.1111/ggr.12494.

Malusà, M. G.; Carter, A.; Limoncelli, M.; Villa, I. M.; Garzanti, E. (2013): Bias in detrital zircon geochronology and thermochronometry. In: *Chemical Geology* 359, pp. 90–107. DOI: 10.1016/j.chemgeo.2013.09.016.

Reiners, P.W. (2005): Zircon (U-Th)/He Thermochronometry. Reviews in Mineralogy & Geochemistry. 58, 151-179, Mineralogical Society of America.

Spiegel, C.; Kohn, B.; Belton, D.; Berner, Z.; Gleadow, A. (2009): Apatite (U-Th-Sm)/He thermochronology of rapidly cooled samples: The effect of He implantation. In: Earth and Planetary Science Letters 285, pp. 105-114.

Vermeesch, P.; Sherlock, S. C.; Roberts, N. M.W.; Carter, A. (2012): A simple method for in-situ U-Th-He dating. In: Geochimica et Cosmochimica Acta 79, pp. 140-147.